Quadruple labelled dual oxygen and pH-sensitive ratiometric nanosensors

Veeren M. Chauhan [a], Francesca Giuntini [b], Jonathan W. Aylott [a],*

[a] Laboratory of Biophysics and Surface Analysis, School of Pharmacy, University of Nottingham, Boots Sciences Building, University Park, Nottingham NG7 2RD, UK
[b] School of Pharmacy & Bimolecular Sciences, James Parsons Building, Liverpool John Moores University, Byrom Street, Liverpool L3 3AF, UK

ABSTRACT

Nanosensors capable of simultaneously measuring dissolved oxygen concentrations from 0 to 100% saturation and pH over the full physiological range, from pH 3.5 to 7.5, that advance the methods towards understanding of key biological gradients, were synthesised. A library of water soluble oxygen-sensitive porphyrins, with three substituted charged functional groups and a chemically flexible carboxylate functional group were spectro-scopically analysed to assess their sensitivity to changes in dissolved oxygen concentrations as free species in solution and in suspension as nanoparticle conjugates. A platinum cationic porphyrin was taken forward to fabricate ratiometric oxygen-sensitive nanosensors, using 5-(and-6)-carboxytetramethylrhodamine (TAMRA) as internal standard. In addition, quadruple labelled dual oxygen and pH-sensitive nanosensors were synthesised using the cationic Pt porphyrin, pH-sensitive fluorescein dyes, carboxyfluorescein (FAM) and Oregon Green (OG), in a 1:1 ratio, and TAMRA. We envisage the dual oxygen and pH nanosensors will find broad utility in the character-isation of diverse microenvironments, where there are complex interactions between molecular oxygen and pH.

1. The elixir of life

Oxygen, the elixir of life [16], is essential for many biological functions [17]. However, the amount of oxygen a biological system is exposed to must be carefully regulated, as too much or too little oxygen can be detrimental to growth and/or disease progression.

At sea level the majority of animals have adapted to breathe air that is composed of 21% oxygen (~21 kPa). The normal oxygen level in human alveoli is approximately 14 kPa [26], which is consumed whilst oxygen is transported throughout the body, via metabolic activity. However, exposure to pure oxygen for extended periods, e.g. during medical treatment, can result in alveolar damage and lung fibrosis [9]. Furthermore, highly metabolising tissue, such as developing embryos, have naturally low oxygen concentration, approximately 5 kPa [26], which is essential for their growth and development. However, uncontrolled increases in oxygen concentration could result in unwanted changes to embryonic stem cell differentiation [20].

Cancer cells proliferate faster than neighbouring tissue consuming large amounts of oxygen very quickly to produce oxygen deficient or hypoxic zones. Highly proliferating cells often have limited blood perfusion, such that they are exposed to low nutrient and oxygen supply, and begin to metabolise via aerobic glycolysis, also known as the "Warburg effect" [23]. Aerobic glycolysis metabolises glucose in an inefficient

manner to produce energy and an acidic by-product. The combination of low oxygen concentration and low pH has been suggested to increase the potential of cancer metastasis and reduce the treatment prognosis for patients with advanced stage cancers [8].

Therefore, real-time measurement of dissolved oxygen, in model systems, could provide an insight into the role oxygen plays in complex biological processes, such as embryo development and cancer. Furthermore, by combining oxygen measurement with other biologically relevant parameters, such as pH, the prognosis of disease treatment could also be improved. For example, we have recently shown how extended dynamic range pH-sensitive nanosensors can be used to monitor real time rhythmic intestinal pH oscillations in the model organism *Caenorhabditis elegans*, to study dyspepsia [4].

In recent years the development of optical oxygen-sensitive sensors that enable accurate quantification of molecular oxygen for measurement in diverse microenvironments has gathered significant momentum [25]. In particular, optical oxygen based nanosensors have attracted attention because: (1) they do not consume oxygen during measurement [12], (2) the optical probes can be dispersed throughout the system of interest with minimal perturbations [28] and are not limited to point-to-point measurement, when compared to the Clark electrode [21], (3) the optical oxygen sensors can be entrapped in a nanoparticle matrix to shield them from measurement interferents, such as emission hindering macromolecules[10], and (4) optical oxygen sensing occurs via collisional quenching of the triplet excited state of oxygen-sensitive phosphors, which takes place as a result of the unique

* Corresponding author.
E-mail address: Jon.Aylott@nottingham.ac.uk (J.W. Aylott).

electronic properties of oxygen, that limit the effects of cross sensitivity with other analytes [27]. To obtain sensitivity at low oxygen concentrations, phosphors with long lifetimes, such as transition metal complexes, are required [5]. Examples of transition metals which have been employed for their utility in oxygen sensing are the ruthenium (II) (Ru) phenanthrolines and the platinum (II) (Pt) and palladium (II) (Pd) metalloporphyrins [19].

This article describes the development of ratiometric oxygen-sensitive nanosensors and quadruple labelled oxygen and pH-sensitive nanosensors using water soluble metalloporphyrins. Cationic and anionic metalloporphyrins were spectrophotometrically assessed for their sensitivity to changes in dissolved oxygen concentrations as free species in solution and in suspensions as nanoparticle conjugates. The best performing metalloporphyrin was taken forward to fabricate oxygen-sensitive nanosensors and quadruple fluorophore labelled dual oxygen and pH-sensitive ratiometric nanosensors. For ratiometric oxygen-sensitive nanosensors a reference fluorophore is assessed for its sensitivity to changes in dissolved oxygen concentration and whether its excitation or emission elicits a phosphorescence response from the metalloporphyrin via energy transfer. Similarly, for the quadruple labelled dual oxygen and pH-sensitive nanosensor both pH-sensitive fluorophores and oxygen-sensitive metalloporphyrin were assessed for their cross sensitivity to oxygen and pH, respectively.
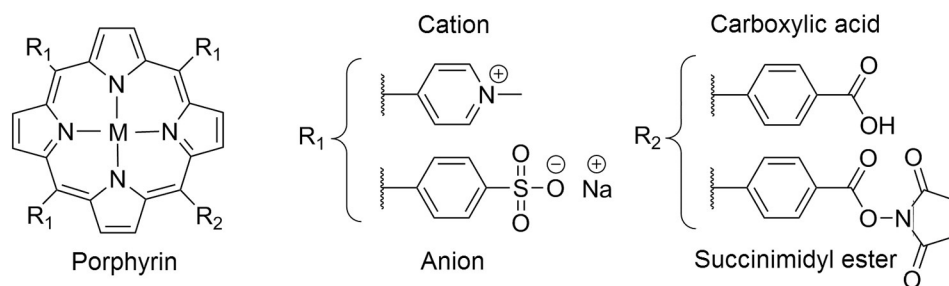
2. Results and discussion

2.1. Development of metalloporphyrins

Porphyrins, containing either a Pt (II) or Pd (II) metal centre, were synthesised through fabrication of substituted porphyrins composed of (1) three substituted charged functional groups and a (2) single chemically flexible carboxylate functional group, as described by Giuntini et al. [7]. Introduction of charged moieties enhances the water solubility of the porphyrins so that they are able to partition into aqueous biological environments. Charged functional groups, in particular cationic moieties, have also been reported to augment delivery of large cargo across the cell membrane [22].

Carboxylate functional groups can be activated by N-hydroxysuccinimide (NHS) for conjugation to primary amines. Introduction of a single activated carboxylate metalloporphyrin, rather than four activated carboxylates, limits the extent of porphyrin crosslinking. This is advantageous, as crosslinking can aggregate porphyrins, which can result in the formation of unwanted precipitates [15] and phosphorescence quenching [2].

Scheme 1 highlights the porphyrin chemical backbone, with substituted charged functional groups and carboxylate functional group positioned at the methine hydrogens. Microwave irradiation was used to add metal centres to the porphyrins. The platinum and palladium metal ion co-ordination geometries are complemented by the cyclic porphyrin structure such that they seldom change their valency and co-ordination state to form stable metalloporphyrins [18].
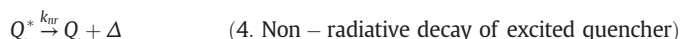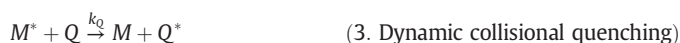
2.2. Oxygen-sensitive phosphorescence response

The phosphorescence response of the oxygen-sensitive metalloporphyrins was determined by bubbling either argon or oxygen gas into a metalloporphyrin solutions, to decrease and increase the dissolved oxygen concentration in the sample, respectively, Fig. 1. For ease of interpretation dissolved oxygen concentrations in this article have been described as percentages of dissolved oxygen concentrations (c %). For biologically relevant measurements these values can be readily converted to alternate measurement units e.g. partial pressures (pO_2) expressed as kPa, Torr, mm Hg or oxygen concentrations (cO_2) expressed as parts per million (ppm), mg/L or μmol/L, using the oxygen concentration conversion equation and Table S1 (see supplementary data).

In the absence of oxygen Pt metalloporphyrins (Fig. 1A & B) were found to exhibit greater than $10\times$ the phosphorescence response when compared to the Pd metalloporphyrins (Fig. 1C & D). Furthermore, the peak phosphorescence response of cationic metalloporphyrins (Fig. 1A & C) with respect to their anionic derivatives in the absence of oxygen is $5.5 \pm 1.4\%$ greater (Fig. 1B & D).

The metalloporphyrins have large Stokes shifts, approximately 280 nm [7]. This adds integrity to oxygen measurements made with these porphyrins as the interference from excitation sources can be eliminated through careful selection of the wavelengths of collected emission. In addition, the large Stokes shift creates a 'window of opportunity' in the visible spectrum, between 450 and 600 nm, to incorporate additional fluorophores in the measurement system (see supplementary data Fig. S1 for absorption measurements).

Normalisation of emission maxima to the peak phosphorescence response in the absence of oxygen permits comparison of the oxygen dependent phosphorescence response of the metalloporphyrins, Fig. 2A. All four metalloporphyrins studied exhibit an exponential decrease in phosphorescence intensity with increases in dissolved oxygen concentration. These observations can be described by the expressions below:

$$M + h\nu_1 \rightarrow M^* \qquad\qquad (1.\ \text{Excitation})$$

$$M^* \xrightarrow{k_r} M + h\nu_2 \qquad\qquad (2.\ \text{Emission})$$

$$M^* + Q \xrightarrow{k_Q} M + Q^* \qquad (3.\ \text{Dynamic collisional quenching})$$

$$Q^* \xrightarrow{k_{nr}} Q + \Delta \qquad (4.\ \text{Non} - \text{radiative decay of excited quencher})$$

where; (1) the metalloporphyrin (M) is excited (to M^*) by photons with energy ($h\nu_1$), (2) the metalloporphyrin relaxes from the excited stated to emit a photon of lower energy ($h\nu_2$) at a rate of k_r, and/or (3) the excited state metalloporphyrin transfers its energy to a quencher, such as oxygen (Q, to form Q^*) through dynamic collisional quenching,

Scheme 1. Chemical structure of substituted metalloporphyrin. Porphyrins can be synthesised with either a platinum (M = Pt) or palladium (M = Pd) centre and triple substituted cationic or anionic water soluble functional groups. The carboxylate functional group positioned at R2 can be activated by N-hydroxysuccinimide to form a succinimidyl ester. The succinimidyl ester provides an excellent leaving group for base catalysed conjugation to primary amines.
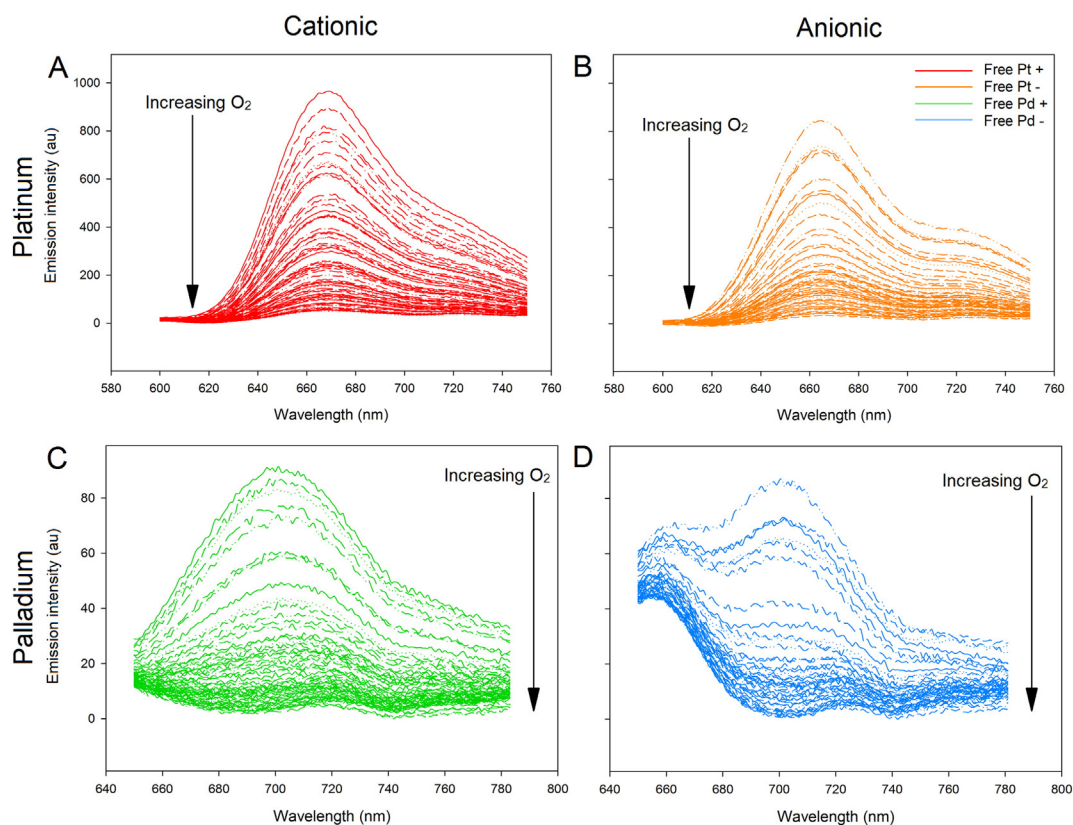
Fig. 1. Emission curves for dissolved oxygen-sensitive (A and B) Pt and (C and D) Pd metalloporphyrins (0.0125 mg/mL) functionalized with (A and C) cationic (+) and (B and D) anionic (−) functional groups in deionised water, when subjected to dissolved oxygen concentrations ranging between 0 and 100%.

such that (4) the excited quencher disperses the extra energy in a non-radiative manner (Δ), *e.g.* through heat or molecular vibrations (at rate k_{nr}) [6,18]. Emission (2) and quenching (3) are competing processes; such that, at a constant metalloporphyrin concentration and excitation, the emission intensity is inversely proportional to the dissolved oxygen concentration, as described by the Stern–Volmer equation:

$$\frac{I_0}{I} = \frac{\tau_0}{\tau} = 1 + K_{sv}[Q] = 1 + k_q.\tau_0[Q] \qquad \text{(5. Stern–Volmer equation)}$$

$$K_{sv} = k_q.\tau_0 \qquad \text{(6. Quenching constant)}$$

where I_0 and I and τ_0 and τ, are unquenched and quenched phosphorescence intensities and phosphorescence lifetimes at oxygen concentration $[Q]$, respectively, and K_{SV} is the Stern–Volmer quenching constant, which describes the sensitivity of fluorophore intensity to quenching by oxygen [12]. The K_{SV} can be determined graphically, by calculating the gradient of a Stern–Volmer plot, or through determination of the product of the bimolecular quenching constant (k_q) and the lifetime of unquenched fluorophore (τ_0).

The Stern–Volmer transformation, Fig. 2B, shows that oxygen effectively quenches the phosphorescence intensity of all four oxygen-sensitive metalloporphyrins, such that the dynamic range of oxygen measurement is extended to the extremes of measurement, from 0 to 100% dissolved oxygen concentrations. In the context of the usability, especially with regard to measurement in biological systems, it is important to note that free metalloporphyrins demonstrate their greatest sensitivity to changes in saturated dissolved oxygen concentration below atmospheric conditions, *i.e.* below 20.95% [11], Fig. 2A. Further analysis of Fig. 2B shows that the Stern–Volmer plots appear to be deviating from linearity at higher oxygen concentrations. This is a common characteristic of Stern–Volmer transformations that are susceptible to static quenching due to non-luminescent dark complex

formation between molecular oxygen and oxygen sensitive-phosphors [13].

2.3. Metalloporphyrin-nanoparticle hybrids

Having demonstrated the oxygen-sensitive response of free metalloporphyrins, metalloporphyrin-nanoparticle hybrids were synthesised to evaluate differences in phosphorescence properties after conjugation to a nanoparticle solid support.

2.3.1. Size and zeta potential characterisation of metalloporphyrin-nanoparticle hybrids
Nanoparticle size, as a function of dynamic light scattering intensity distributions, ranged from 10 to 100 nm such that modal nanoparticle size increases in the order Pt (−) < Pd (−) < Pd (+) < Pt (+) < Blank (see supplementary data Fig. S2 and Table S3).

The zeta potentials for the Pt and Pd metalloporphyrins, bearing cationic and anionic functional groups, and blank unfunctionalised nanoparticles are shown in Fig. 3. In general, the metalloporphyrin functionalised nanoparticles demonstrate an increase in zeta potential as the pH of the suspending media is reduced from pH 8.0 to 3.0. Whereas, the zeta potential for blank unfunctionalised nanoparticles does not change with pH, but maintains a partial negative zeta potential over the same pH range, − 1.18 ± 0.33 mV. Primarily this observation indicates that functionalisation of nanoparticle matrices with metalloporphyrins has resulted in the nanoparticles acquiring a charge.

Secondly, by focussing on the zeta potentials at pH 7.5, which corresponds to the physiological pH (~7.4), cationic platinum porphyrins possess a greater positive zeta potential than cationic palladium porphyrins (Pt (+) mV > Pd (+) mV), whilst the anionic palladium porphyrins possess a greater negative zeta potential when compared to anionic platinum porphyrins (Pd (−) mV > Pt (−) mV). Therefore, metalloporphyrins composed of a Pt centre demonstrate a more
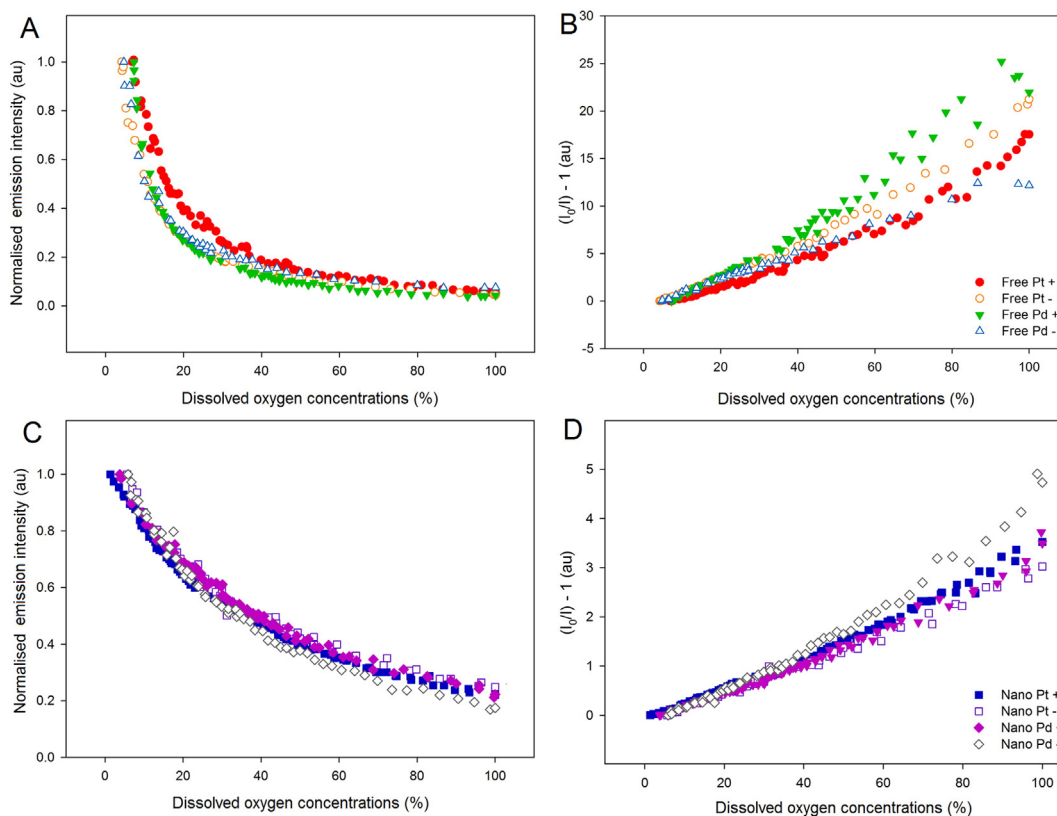
Fig. 2. (A) Normalised emission response and (B) Stern–Volmer transformations for free platinum (Pt) and palladium (Pd) porphyrins functionalized with positive (+) and negative (−) function groups, when subjected to dissolved oxygen concentration ranging between 0% and 100%. (C) Normalised phosphorescence response and (D) Stern–Volmer transformations for free and nanoparticle conjugated Pt and Pd metalloporphyrins, functionalized with cationic (+) and anionic (−) function groups, when subjected to dissolved oxygen concentrations ranging between 0 to 100%.

positive zeta potential than their corresponding cationic or anionic palladium metalloporphyrins. This is important as nanoparticles that possess a positive zeta potential, such as the cationic platinum nanoparticles shown here, have been shown to augment intracellular delivery [14].
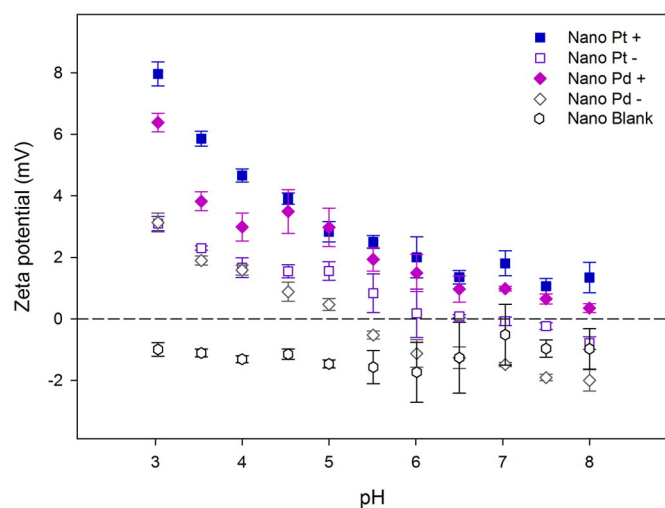

Fig. 3. Zeta potentials for cationic (+) and anionic (−) Pt and Pd metalloporphyrin functionalized nanoparticles and unfunctionalised blank nanoparticles suspended in buffer solutions ranging from pH 8.0 to 3.0 (n = 3).

2.3.2. Spectroscopic properties of oxygen-sensitive metalloporphyrin nanoparticles

The oxygen dependent phosphorescence response of metalloporphyrin conjugated nanoparticles was investigated through suspension of the nanoparticles in deionised water at identical concentrations (0.5 mg/mL), Fig. 2C. The K_{SV} for free metalloporphyrins compared to nanoparticle conjugated metalloporphyrins is approximately 5 times greater, Fig. 2B and D, respectively. These reduced quenching effects have been attributed to the nanoparticle matrix, which shields the metalloporphyrins from dynamic collisional quenching and static quenching due to non-luminescent dark complex formation between molecular oxygen and oxygen sensitive-phosphor [13]. This has led to the metalloporphyrin nanoparticle hybrids reported here exhibiting an emission response that produces a Stern–Volmer plot with enhanced linearity, Fig. 2D. As a result the emission response of metalloporphyrin-nanoparticle hybrids, when compared to free phosphors, Fig. 2B, permits effective quantification of dissolved oxygen over the full dynamic range.

The cationic platinum porphyrin was taken forward as the metalloporphyrin of choice because (1) it demonstrates approximately ten times greater phosphorescence intensity than the palladium porphyrins at identical concentrations, Fig. 1, (2) it possesses a positive zeta potential, Fig. 3, which has been shown to augment intracellular delivery [22] and (3) it exhibits a superior k_q of, 6.39×10^8 M^{-1}s^{-1} [7], when compared to Pt (−), Pd (−) and Pd (+) metalloporphyrin conjugated nanoparticles.

2.4. Ratiometric oxygen-sensitive nanoparticles

Ratiometric oxygen-sensitive nanoparticles were fabricated by conjugating amino functionalised polyacrylamide nanoparticles to the

cationic Pt metalloporphyrin succinimidyl ester (SE) and 5-(and-6)-carboxytetramethylrhodamine (TAMRA) SE. The fluorescence excitation and emission of TAMRA lie within the "window of opportunity" of the metalloporphyrins, at 540 nm and 577 nm, respectively, which does not interfere/crossover with the metalloporphyrin's oxygen dependent fluorescence signal. In addition, the fluorescence emission of TAMRA was found to be insensitive to changes in dissolved oxygen concentrations (see supplementary data Fig. S3A & B). Nanoparticles with diameters ranging from 10 to 100 nm were synthesised with a modal particle diameter of 34 nm (PDI = 0.16), measured using dynamic light scattering. The nanoparticles also held a zeta potential of 2.05 ± 0.34 mV (pH 7.5).

When the ratiometric oxygen-sensitive nanosensors are excited at 400 nm, the nanosensors emit fluorescence and phosphorescence signals corresponding to oxygen-insensitive TAMRA (577 nm) and oxygen-sensitive cationic platinum metalloporphyrin (670 nm), respectively, Fig. 4A. By taking a ratio of the peak response of the oxygen-sensitive metalloporphyrin to the oxygen-insensitive TAMRA (λ_{em} 670 nm/λ_{em} 577 nm), a ratiometric calibration curve can be generated, Fig. 4B left axis, which can then be transformed into a ratiometric Stern–Volmer plot, Fig. 4B right axis. The Stern–Volmer transformation demonstrates a linear phosphorescence response over a dissolved oxygen concentration range of 0% to 100% saturation. The K_{SV} of 0.0047 mm Hg^{-1} (0.0375%$^{-1}$) is comparable to the K_{SV} of the non-ratiometric platinum metalloporphyrin conjugated nanoparticles, of 0.0051 mm Hg^{-1} (0.0347%$^{-1}$), Fig. 2D.
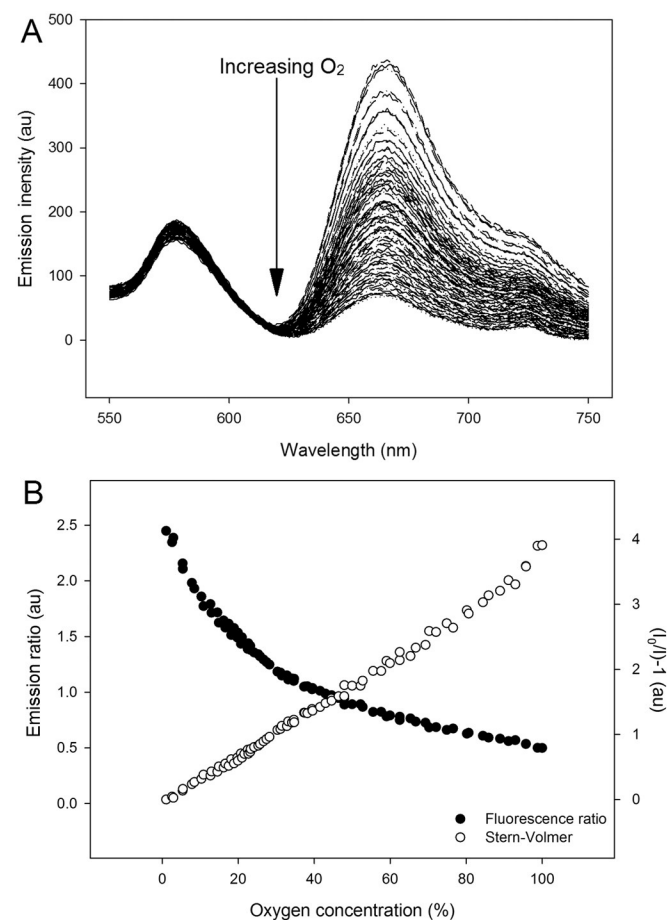

Fig. 4. (A) Emission curves for ratiometric oxygen-sensitive nanosensors composed of cationic Pt metalloporphyrin and oxygen-insensitive fluorophore TAMRA, (λ_{ex} 400 nm). (B) Emission ratio (left axis) and ratiometric Stern–Volmer transformation (right axis) for ratiometric oxygen-sensitive nanosensors, when subjected to dissolved oxygen concentrations ranging from 0% to 100% ($R^2 = 0.99$).

2.5. Quadruple labelled dual oxygen and pH-sensitive ratiometric nanosensors

The ratiometric oxygen sensor described in the previous section highlights how the large Stokes shifts of the metalloporphyrins allow for the synthesis of a ratiometric nanoparticle though use of a TAMRA oxygen-insensitive fluorophore. This "window of opportunity" was utilised to incorporate additional fluorophores, such as the fluoresceins carboxyfluorescein (FAM) and Oregon Green® (OG), which excite and emit between 400 nm and 540 nm, to synthesise a dual oxygen and pH-sensitive ratiometric quadruple labelled nanosensor. We have previously shown nanosensors incorporating FAM and OG in a 1:1 ratio in polyacrylamide nanoparticles, alongside TAMRA as a reference fluorophore, can be used to make pH measurements over the full physiological pH range, from 3.5 to 7.5 [3]. Using an analogous approach, dual oxygen and pH-sensitive ratiometric nanosensors were prepared by conjugating Pt cationic porphyrin-SE, TAMRA-SE, FAM-SE and OG-SE to amino functionalised nanoparticles. Covalent attachment of all indicator and reference dyes directly to the nanoparticle architecture eliminates measurement artefacts due to dye leaching [1,24]. Nanosensors with diameters ranging between 10 and 100 nm were synthesised, with a modal nanoparticle diameter of 56 nm (PDI = 0.21), and of zeta potential of 2.32 ± 0.13 mV (pH 7.5). To explore the ability to simultaneously sense pH and oxygen (1) the pH response of the dual sensors was investigated at high and low dissolved oxygen concentrations, and (2) the oxygen response was investigated at pH 8.0 and 3.0 using fluorescence spectroscopy.

The pH response of the dual sensors, suspended in buffer solutions ranging from pH 8.0 to 3.0, was investigated at low (0%) and high (100%) dissolved oxygen concentrations, Fig. 5A & B. Examination of the peak fluorescence ratio of the fluorescein derivatives and TAMRA (λ_{em} 520 nm/λ_{em} 577 nm), show that there is no observable difference in the fluorescence response and calibration curves at high and low dissolved oxygen concentrations, Fig. 5C. The effect of pH on the oxygen response of dual sensors was investigated by determining the change in phosphorescence intensity of the metalloporphyrins at different dissolved oxygen concentrations at pH 8.0 and pH 3.0, Fig. 5D & E. Ratiometric analysis of the metalloporphyrin and TAMRA emission maxima (λ_{em} 670 nm/λ_{em} 577 nm) and ratiometric Stern–Volmer transformations highlights that the oxygen response of the metalloporphyrins is not affected by the pH of the suspending media, Fig. 5F. The cross-insensitivity of the pH and oxygen-sensitive indicators to oxygen and pH, respectively, was also confirmed using fluorescence microscopy (see supplementary data Fig. S4).

3. Conclusion

In summary, we have demonstrated the synthesis and characterisation of ratiometric oxygen-sensitive nanosensors and quadruple labelled dual oxygen and pH-sensitive ratiometric nanosensors. The oxygen sensitive phosphor was selected by spectroscopically surveying a library of Pt and Pd metalloporphyrins. A cationic Pt metalloporphyrin was used to synthesise ratiometric oxygen-sensitive nanosensors incorporating TAMRA as a reference fluorophore. Dual oxygen and pH-sensitive ratiometric nanosensors were produced by combining the pH-sensitive fluoresceins, FAM and OG, the oxygen-sensitive Pt cationic metalloporphyrin and the oxygen and pH-insensitive fluorophore TAMRA. The fluoresceins did not exhibit a change in their fluorescence response to changes in dissolved oxygen concentration; furthermore the metalloporphyrin upheld its response to changes in oxygen concentration at both high and low pH.

The quadruple dye labelled dual oxygen and pH-sensitive ratiometric nanosensors detailed in this article are capable of measuring dissolved oxygen concentrations, from 0 to 100%, and the full physiological pH ranges from pH 3.5 to 7.5. We envisage that dual oxygen and pH
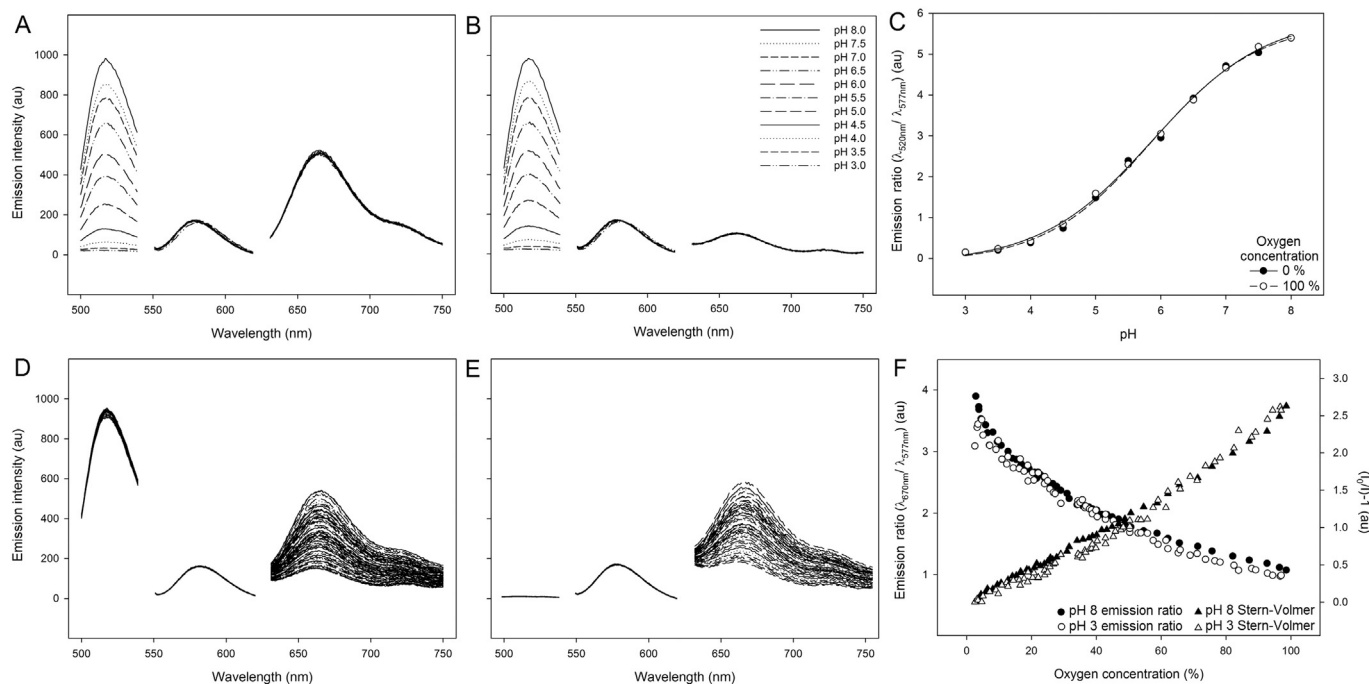
Fig. 5. Emission curves comparing the pH fluorescence intensity in the (A) absence and (B) presence of oxygen for dual oxygen, and pH-sensitive nanosensors. (C) pH calibration curve for dual oxygen and pH-sensitive nanosensors in the absence and presence of oxygen (pK_a's of pH 5.86 ± 0.02). Emission curves comparing the oxygen phosphorescence intensity at (D) pH 8.0 and (E) pH 3.0, for dual oxygen and pH-sensitive nanosensors. (F) Emission ratio (left axis) and ratiometric Stern–Volmer transformation (right axis) calibration curves for dual oxygen and pH-sensitive nanosensors at pH 8.0 and 3.0.

nanosensor will find potential utility in the characterisation of diverse microenvironments, especially where there is interplay between pH and dissolved oxygen concentrations, such as, developing embryos and cancer tumours.

4. Experimental

Control and measurement of dissolved oxygen concentrations — dissolved oxygen concentrations were measured using an Ocean Optics NeoFox (NFB0181) phosphorescence-based optical sensor probe. The phosphorescence lifetime of the probe can be calibrated to 0% and 100% dissolved oxygen concentrations.

The calibrated probe was immersed in solutions of metalloporphyrins (0.01 mg/mL, 10 mL) and suspensions of oxygen-sensitive nanoparticles (0.50 mg/mL, 10 mL) in deionised water. The dissolved oxygen concentration of these solutions/suspensions was varied by bubbling in argon and oxygen gas, representing 0% and dissolved 100% oxygen concentration, respectively. Oxygen-dependent emission intensities of samples (1 mL) were recorded using a Varian Cary Eclipse fluorescence spectrophotometer.

For dissolved oxygen concentrations below atmospheric oxygen concentrations stirring samples were deoxygenated by bubbling in argon gas. Once the samples were deoxygenated the argon source was removed and the samples were allowed to equilibrate to atmospheric oxygen concentrations. For dissolved oxygen concentrations above atmospheric oxygen concentrations stirring samples were oxygenated by bubbling in oxygen gas. Once the samples were fully oxygenated the oxygen source was removed and the samples were allowed to equilibrate to atmospheric oxygen concentrations. Emission spectra of equilibrating samples were taken at regular intervals, from which an oxygen-dependent emission response was determined.

Ratiometric oxygen-sensitive nanosensors (0.5 mg/mL), composed of cationic platinum metalloporphyrin and oxygen-insensitive fluorophore TAMRA were excited at a single wavelength (400 nm) and emission was collected between 540 and 700 nm (slit size 10 nm). For dual oxygen

and pH-sensitive nanosensors each fluorophore/phosphor was excited at their own excitation wavelengths and slit sizes, to determine their luminescence properties; for example, the fluorescein derivatives (FAM and OG), TAMRA and the Pt metalloporphyrins were excited at 488 nm (2.5 nm slit size), 540 nm (5.0 nm slit size) and 405 nm (10.0 nm slit size), whereas their emission spectra were collected between 500–540 nm (5.0 nm slit size), 550–620 nm (5.0 nm slit size), and 630–750 nm (20.0 nm slit size), respectively.

Zeta potential — Pt and Pd oxygen-sensitive and blank unfunctionalised nanoparticles were suspended (0.5 mg/mL) in filtered pH buffer solutions (0.02 μm, Millipore). Buffer solutions were prepared to cover the full physiological pH range, from 3.0 to 8.0 using mixtures of sodium phosphate dibasic (0.2 M) and citric acid monohydrate (0.1 M). Nanoparticle suspensions were transferred to zetasizer cuvettes (DTS1061, Malvern), flushed with filtered deionised water. Zeta potential measurements were made in triplicate for each nanoparticle suspension at each pH (constants used to make measurements for polyacrylamide nanoparticles: refractive index: 1.452, parameters used for dispersant deionised water dispersant; refractive index: 1.330, viscosity: 0.8872 cP, dielectric constant: 78.5 εr, Model Smoluchowski F (K_a) 1.5). All samples were allowed to equilibrate to 25 °C for 120 s prior to measurement.

Author contributions

VMC wrote the article and supplementary data; prepared figures; analysed data; designed and performed spectroscopic and microscopic experiments for analysis of free metalloporphyrins, metalloporphyrin functionalised nanoparticles, ratiometric oxygen-sensitive nanosensors and quadruple labelled oxygen and pH-sensitive nanosensors; characterised nanoparticles for size and zeta potential. FG designed, synthesised and characterised cationic and anionic Pt and Pd metalloporphyrins. All authors contributed to scientific planning, direction and discussion.

Acknowledgements

Appendix A. Supplementary data

A detailed list of materials and experimental methods for (1) synthesising oxygen-sensitive metalloporphyrins, (2) preparation of amino functionalised nanoparticles (3) attachment of fluorescent and phosphorescent to amino functionalised nanoparticle matrices (4) metalloporphyrin absorption measurements are detailed in the supplementary data. In addition, results highlighting (1) porphyrin absorption measurements (2) modal size and for metalloporphyrins (3) sensitivity of TAMRA and fluoresceins (FAM and OG) to changes in dissolved oxygen concentrations and (4) study of nanosensor response using fluorescence microscopy are also shown in the supplementary data. Supplementary data associated with this article can be found in the online version, at http://dx.doi.org/10.1016/j.sbsr.2016.03.007.

References

[1] K. Almdal, H. Sun, A.K. Poulsen, L. Arleth, I. Jakobsen, H. Gu, A.M. Scharff-Poulsen, Fluorescent gel particles in the nanometer range for detection of metabolites in living cells, Polym. Adv. Technol. 17 (9–10) (2006) 790–793.
[2] S.B. Brown, M. Shillcock, P. Jones, Equilibrium and kinetic studies of aggregation of porphyrins in aqueous-solution, Biochem. J. 153 (2) (1976) 279–285.
[3] V.M. Chauhan, G.R. Burnett, J.W. Aylott, Dual-fluorophore ratiometric pH nanosensor with tuneable pK(a) and extended dynamic range, Analyst 136 (9) (2011) 1799–1801.
[4] V.M. Chauhan, G. Orsi, A. Brown, D.I. Pritchard, J.W. Aylott, Mapping the pharyngeal and intestinal pH of Caenorhabditis elegans and real-time luminal pH oscillations using extended dynamic range pH-sensitive nanosensors, ACS Nano 7 (6) (2013) 5577–5587.
[5] J.N. Demas, B.A. Degraff, Design and applications of highly luminescent transition-metal complexes, Anal. Chem. 63 (17) (1991) A829–A837.
[6] J.N. Demas, B.A. DeGraff, P.B. Coleman, Oxygen sensors based on luminescence quenching, Anal. Chem. 71 (23) (1999) 793A–800A.
[7] F. Giuntini, V.M. Chauhan, J.W. Aylott, G.A. Rosser, A. Athanasiadis, A. Beeby, A.J. MacRobert, R.A. Brown, R.W. Boyle, Conjugatable water-soluble Pt(II) and Pd(II) porphyrin complexes: novel nano-and molecular probes for optical oxygen tension measurement in tissue engineering, Photochemical & Photobiological Sciences 13 (7) (2014) 1039–1051.
[8] M. Hockel, C. Knoop, K. Schlenger, B. Vorndran, E. Baussmann, M. Mitze, P.G. Knapstein, P. Vaupel, Intratumoral pO$_2$ predicts survival in advanced cancer of the uterine cervix, Radiother. Oncol. 26 (1) (1993) 45–50.
[9] A.L.A. Katzenstein, C.M. Bloor, A.A. Leibow, Diffuse alveolar damage — role of oxygen, shock, and related factors — review, Am. J. Pathol. 85 (1) (1976) 210-&.
[10] Y.E.L. Koo, R. Agayan, M.A. Philbert, A. Rehemtulla, B.D. Ross, R. Kopelman, Photonic Explorers Based on Multifunctional Nanoplatforms: In Vitro and in Vivo Biomedical Applications, in: K. Kneipp, R. Aroca, H. Kneipp, E. Wen trupByrne (Eds.), New Approaches in Biomedical SpectroscopyAm. Chem. Soc., Washington 2007, pp. 200–218.
[11] H. Kurokawa, H. Ito, M. Inoue, K. Tabata, Y. Sato, K. Yamagata, S. Kizaka-Kondoh, T. Kadonosono, S. Yano, M. Inoue, T. Kamachi, High resolution imaging of intracellular oxygen concentration by phosphorescence lifetime, Scientific Reports 5 (2015).
[12] J.R. Lakowicz, Principles of Fluorescence Microscopy, second ed. Kluwer Academic/ Plenum Publishers, New York, 1999.
[13] J.R. Lakowicz, G. Weber, Quenching of fluorescence by oxygen — probe for structural fluctuations in macromolecules, Biochemistry 12 (21) (1973) 4161–4170.
[14] A.S. Lavado, V.M. Chauhan, A.A. Zen, F. Giuntini, D.R.E. Jones, R.W. Boyle, A. Beeby, W. Chan, J.W. Aylott, Controlled intracellular generation of reactive oxygen species in human mesenchymal stem cells using porphyrin conjugated nanoparticles, Nanoscale (2015).
[15] S.P. Martsev, V. Preygerzon, Y.I. Melnikova, Z.I. Kravchuk, G.V. Ponomarev, V.E. Lunev, A.P. Savitsky, Modification of monoclonal and polyclonal igg with palladium(ii) coproporphyrin-i — stimulatory and inhibitory functional-effects induced by 2 different methods, J. Immunol. Methods 186 (2) (1995) 293–304.
[16] L. Nick, Oxygen: The Molecule That Made the World, Oxford University Press, 2003.
[17] P.R. Ogilby, Singlet oxygen: there is indeed something new under the sun, Chem. Soc. Rev. 39 (8) (2010) 3181–3209.
[18] D.B. Papkovsky, Methods in optical oxygen sensing: protocols and critical analyses, Oxygen Sensing 381 (2004) 715–735.
[19] M. Quaranta, S.M. Borisov, I. Klimant, Indicators for optical oxygen sensors, Bioanal. Rev. 4 (2–4) (2012) 115–157.
[20] M.C. Simon, B. Keith, The role of oxygen availability in embryonic development and stem cell function, Nat. Rev. Mol. Cell Biol. 9 (4) (2008) 285–296.
[21] J.R. Stetter, J. Li, Amperometric gas sensors — a review, Chem. Rev. 108 (2) (2008) 352–366.
[22] H.H. Sun, T.L. Andresen, R.V. Benjaminsen, K. Almdal, Polymeric nanosensors for measuring the full dynamic pH range of endosomes and lysosomes in mammalian cells, J. Biomed. Nanotechnol. 5 (6) (2009) 676–682.
[23] M.G. Vander Heiden, L.C. Cantley, C.B. Thompson, Understanding the Warburg effect: the metabolic requirements of cell proliferation, Science (New York, N.Y.) 324 (5930) (2009) 1029–1033.
[24] X.-d. Wang, J.A. Stolwijk, T. Lang, M. Sperber, R.J. Meier, J. Wegener, O.S. Wolfbeis, Ultra-small, highly stable, and sensitive dual nanosensors for imaging intracellular oxygen and pH in Cytosol, J. Am. Chem. Soc. 134 (41) (2012) 17011–17014.
[25] X.D. Wang, O.S. Wolfbeis, Optical methods for sensing and imaging oxygen: materials, spectroscopies and applications, Chem. Soc. Rev. 43 (10) (2014) 3666–3761.
[26] J.P.T. Ward, Oxygen sensors in context, Biochimica Et Biophysica Acta-Bioenergetics 1777 (1) (2008) 1–14.
[27] X.D. Wu, Y. Cong, Y.H. Liu, J. Ying, B. Li, Luminescence and oxygen sensing properties of ORMOSILs covalently grafted with a novel ruthenium(II) complex, Journal of Sol–Gel Science and Technology 49 (3) (2009) 355–363.
[28] H. Xu, J.W. Aylott, R. Kopelman, T.J. Miller, M.A. Philbert, A real-time ratiometric method for the determination of molecular oxygen inside living cells using sol–gel-based spherical optical nanosensors with applications to rat C6 glioma, Anal. Chem. 73 (17) (2001) 4124–4133.